



Interseismic re-strengthening and stabilization of carbonate faults by “non-Dieterich” healing under hydrothermal conditions



Jianye Chen^{a,b,*}, Berend A. Verberne^b, Christopher J. Spiers^b

^a State Key Laboratory of Earthquake Dynamics, Institute of Geology, China Earthquake Administration, Beijing, China

^b HPT Laboratory, Department of Earth Sciences, Utrecht University, The Netherlands

ARTICLE INFO

Article history:

Received 29 July 2014

Received in revised form 14 March 2015

Accepted 16 March 2015

Available online 29 April 2015

Editor: A. Yin

Keywords:

frictional healing

slip stabilization

carbonate gouge

hydrothermal conditions

ABSTRACT

Friction experiments, consisting of a “velocity stepping” stage, a “slide-hold-slide” (SHS) stage and a second “velocity stepping” stage, have been performed to study the frictional healing behavior of carbonate fault gouge, and the effects of healing on the velocity dependence of friction, at 20–140 °C and at 50 MPa effective normal stress. Dry experiments show classical Dieterich healing characterized by a transient peak in friction after each hold period, with no effects of SHS testing on steady-state friction or velocity dependence. By contrast, the wet tests show 1) an increase in apparent steady-state friction upon re-sliding after a hold period, and 2) a pronounced increase in the velocity dependence parameter, $(a - b)$, after the SHS stage. While the first of these “non-Dieterich-type” healing effects has been observed in previous hydrothermal experiments on simulated quartz gouges, it has not been reported previously for carbonate gouges. The observed effect of SHS-testing on $(a - b)$ has never been reported. Our findings suggest that, under in-situ hydrothermal conditions, interseismic fluid-assisted deformation processes, such as pressure solution, can significantly promote fault re-strengthening in carbonates and can cause slip stabilization. If the results are applicable to active faults in carbonate terrains, they have important implications for understanding how the extent of the seismogenic zone, and how earthquake magnitude and aftershock distributions, may evolve with repeated cycles of natural seismicity and interseismic healing.

© 2015 Elsevier B.V. All rights reserved.

1. Introduction

Most moderate to large earthquakes occurring in the continental crust nucleate in crystalline basement at depths of ~10–25 km, i.e. in the brittle-plastic transitional region for silicate rock types (Sibson, 1982). As a result, most experimental work has focused on characterizing frictional properties relevant to these materials under the corresponding P-T-Stress conditions (e.g. Dieterich, 1979; Blanpied et al., 1995; He et al., 2007). However, in tectonically active regions dominated by carbonate cover lithologies, destructive earthquake ruptures commonly nucleate and/or propagate at shallower depth, i.e. in the upper 5–15 km of the crust (Mirabella et al., 2008). Examples include the 1995 Mw 6.2 Aigion earthquake in Greece (hypocentral depth 7.2 km, Bernard et al., 2006), the 2009 Mw 6.3 L'Aquila earthquake in Italy (9.5 km, Chiarabba et al., 2009), and the 2008 Mw 7.9 Wenchuan earthquake in China

(11 km for the north segment, Xu et al., 2009). Recent experimental studies (e.g. Verberne et al., 2010) have shown that shallow seismicity, characterized by significant stress drops, is likely to be promoted in such terrains because carbonate fault rocks are strong (friction coefficient of ~0.7) and prone to unstable slip at relatively low P-T conditions. For this reason, and because of the need for improved seismic hazard evaluation in carbonate terrains such as those mentioned above, the frictional properties of carbonate faults are attracting increased attention in relation to earthquake nucleation and rupture propagation (e.g. Han et al., 2007; Verberne et al., 2013a). Specific points of interest include the frictional strength of carbonate fault gouges, their rate-and-state dependent friction (RSF) behavior and the underlying microphysical processes that control in-situ fault friction. To date, however, data on carbonate fault friction remain sparse, especially regarding the effects of fluids at in-situ, seismogenic, P-T conditions, where solution-transfer and other thermally-activated processes operate. Most experiments that have been reported have been conducted at coseismic slip rates (e.g. Han et al., 2007; De Paola et al., 2011), with only a few studies addressing carbonate fault friction in the rupture nucleation regime (Verberne et al., 2013a; Scuderi et al., 2013; Carpenter et al., 2014). In particular, very lit-

* Corresponding author at: State Key Laboratory of Earthquake Dynamics, Institute of Geology, China Earthquake Administration, Beijing, China. Tel.: +86 10 62009030; fax: +86 10 62009030.

E-mail address: jyichen@ies.ac.cn (J. Chen).

Type 1a healing
(Dieterich-type with $\Delta\mu_{pk} = \Delta\mu_w = \beta \log(1+t_h/t_c)$)

or **Type 1b healing**
(non-Dieterich-type with $\Delta\mu_{pk} = \Delta\mu_w \neq \beta \log(1+t_h/t_c)$)

Type 2 healing
(non-Dieterich-type with $\Delta\mu_{pk} > \Delta\mu_w$)

Type 3 healing
(non-Dieterich-type with $\Delta\mu_{pk} < \Delta\mu_w$)

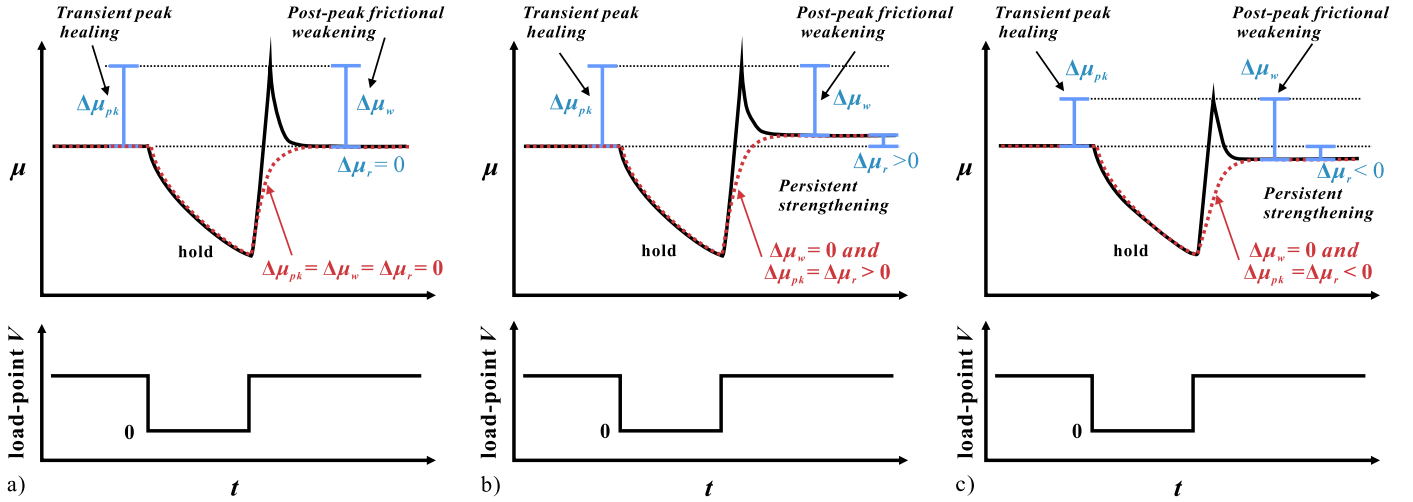


Fig. 1. Definition of frictional healing parameters obtained in SHS tests, as required to describe all possible phenomenological classes of healing behavior (Dieterich- and non-Dieterich-types, see text), which can be generally classified into 3 types shown in (a), (b) and (c), respectively. Note the inequality in Type 1b means that $\Delta\mu_{pk}$ is not well described by a log-linear relationship of the type found by Dieterich (1979), i.e. better described by other functions, as sometimes reported in the literature (e.g. power law, Coulomb, 1785). The healing behaviors indicated by the red dotted lines, characterized by a zero slip-weakening effect ($\Delta\mu_w = 0$), have also been previously reported, mostly at high temperatures (e.g. Olsen et al., 1998), and phyllosilicate-rich gouges (Carpenter et al., 2011). See Supplementary material for details.

tle is known about the interseismic (re)strengthening or healing behavior of carbonate faults, though such data are crucial for understanding the seismic cycle and its repeat frequency.

In silicate rock systems, fault healing and associated strength recovery effects have been widely investigated in relation to both natural (Li et al., 2003; Marone et al., 1995) and laboratory earthquakes (e.g. Wong and Zhao, 1990). These effects strongly influence earthquake nucleation and magnitude, as well as recurrence intervals (e.g. Ruina, 1983; Marone, 1998b). In the classical framework of RSF modeling, frictional healing, i.e. the transient strengthening effect measured in a so-called slide-hold-slide (SHS) experiment, is treated as increasing linearly with the logarithm of “hold time” (Dieterich, 1979). Such time-dependent fault re-strengthening, or “Dieterich-type” healing behavior, is commonly assumed in modeling fault behavior during the seismic cycle. However, the relevance of this behavior to natural faults has recently been questioned on the basis of healing experiments conducted on quartz fault rocks under hydrothermal conditions (Karner et al., 1997; Olsen et al., 1998; Nakatani and Scholz, 2004; Tenthorey and Cox, 2006). These studies have shown that the operation of thermally activated and/or fluid-assisted deformation mechanisms, such as pressure solution, can significantly enhance re-strengthening processes in quartz, far beyond the values predicted by the Dieterich-type log-linear aging law. However, no data are yet available on the potential importance of such effects in carbonates, or on the microphysical mechanisms responsible for healing in carbonates.

In an attempt to fill this knowledge gap, we investigate the slip stability and healing behavior of simulated carbonate fault gouge sheared at temperatures ranging from 20 to 140 °C, at effective normal stress of 50 MPa, under both dry and wet conditions. While the dry experiments show classical Dieterich-type healing behavior (e.g. Marone, 1998b), the wet experiments show enhanced or “non-Dieterich-type” healing effects, as well as healing-induced changes in the velocity dependence of frictional strength that have not been recognized previously. Our observations cannot be described or explained in terms of standard RSF concepts of healing, and lead to an alternative conceptual model for healing effects in

carbonate faults with potentially important implications for seismicity in carbonate terrains.

2. Definitions used in this study

The experimental method used here, and in previous work on fault healing, is the slide-hold-slide (SHS) method. To describe the SHS healing behavior observed reported here and in previous, mainly hydrothermal experiments on silicates (e.g. Nakatani and Mochizuki, 1996; Karner et al., 1997; Yasuhara et al., 2005; Niemeijer et al., 2008; Tenthorey and Cox, 2006), three strength change parameters are ideally required. Here we use the three defined in Fig. 1. These allow description of all possible “Dieterich-type” and “non-Dieterich-type” healing (DH and NDH) responses. In this scheme, $\Delta\mu_{pk}$ represents the transient peak strength increase due to healing, measured in terms of the difference between the peak friction upon re-shearing and the pre-hold steady-state friction coefficient. By contrast, $\Delta\mu_w$ is the post-peak frictional weakening, measured as the difference between the peak and the post-hold steady-state friction coefficients. Lastly, $\Delta\mu_r = (\Delta\mu_{pk} - \Delta\mu_w)$, is the residual, persistent strengthening, measured as the change in quasi steady-state friction coefficient values observed after vs. before the hold period. This describes an increase in apparent steady-state strength that is not erased in the post-hold slip distances investigated, which are similar here to the slip distances of 0.2–0.5 mm investigated in most previous SHS work (e.g. Yasuhara et al., 2005). Making use of these parameters and taking into account the way in which they depend on hold time (t_h) in previous healing studies, we now distinguish the following generically possible categories of frictional healing response to SHS testing (see Fig. 1 and Supplementary material):

1) Type 1 healing. In this type, $\Delta\mu_{pk} = \Delta\mu_w$ and $\Delta\mu_r = 0$ (Fig. 1a). Two subclasses can then be defined:

Type 1a healing (Classical DH). Here $\Delta\mu_{pk} = \Delta\mu_w = \beta \log(1 + t_h/t_c)$, where t_c is cutoff time of ~ 1 s, so that at long times

$\Delta\mu_{pk} = \Delta\mu_w = \beta \log(t_h)$ and $\beta = d(\Delta\mu_{pk})/d \log(t_h)$ is a constant known as the healing rate.

Type 1b healing (NDH). In this case, the logarithmic relation is not obeyed and $\Delta\mu_{pk}$ can be any other function of hold time.

2) Type 2 healing (NDH). Here, $\Delta\mu_{pk} > \Delta\mu_w$ and $\Delta\mu_r > 0$ (Fig. 1b). In addition, we may have $\Delta\mu_x = \beta_x \log(1 + t_h/t_c)$ or any other function of t_h , where $\Delta\mu_x$ represents $\Delta\mu_{pk}$, $\Delta\mu_w$ or $\Delta\mu_r$, and where $\beta_x = d(\Delta\mu_x)/d \log(t_h)$.

3) Type 3 healing (NDH). As a last possibility, $\Delta\mu_{pk} < \Delta\mu_w$ and $\Delta\mu_r < 0$ (Fig. 1c). As in Type 2 healing, any function of $\Delta\mu_x$ versus t_h could apply here.

3. Experimental material and method

The starting material used for our experiments consisted of carbonate fault breccia collected from a surface exposure of the Yingxiu–Beichuan fault, which hosted the devastating 2008 M_w 7.9 Wenchuan earthquake in Sichuan, China. The exposure studied is located ~ 3 km away from the point of the largest coseismic surface displacement (~ 11 m, P. Zhang et al., 2010), in a region where the coseismic rupture cut through extensive carbonate rocks (Chen et al., 2013). A representative sample of fault breccia, taken from this exposure, was crushed and then sieved using a 35 μ m sieve, to produce a simulated fault gouge. X-ray diffraction analyses showed that the simulated gouge consisted of 68% calcite, 29% dolomite, 1% quartz, and 2% clays (mainly mixed layer smectite–illite).

We conducted friction experiments on 1 mm thick layer of the simulated fault gouge using the internally heated, pressure-compensated, triaxial testing apparatus plus direct shear assembly described by Verberne et al. (2013b). The direct shear assembly used in the experiments consisted of a “69” forcing-block configuration specially designed for use in triaxial testing machines (see Fig. 2 and Supplement).

In total, we ran 9 experiments (Table 1), comprising three dry and six wet tests, at temperatures (T) of $\sim 20^\circ\text{C}$, 80°C and 140°C , all at 50 MPa effective normal stress (σ_n). Wet tests were performed under drained conditions, using a fluid pressure of 15 MPa and a confining pressure of 65 MPa. Pore fluid pressure was controlled, and sample pore volume changes measured, using a high precision, servo-controlled volumetric pump. Dry samples were drained to lab air. As illustrated in Fig. 3, in each run we applied a total shear displacement of 5 to 6 mm, divided into the following stages: 1) slip at an initially constant “run-in” displacement rate of $V = 1$ or 10 $\mu\text{m/s}$, imposed until a steady-state frictional strength was reached, 2) a velocity stepping sequence, 3) a slide-hold-slide

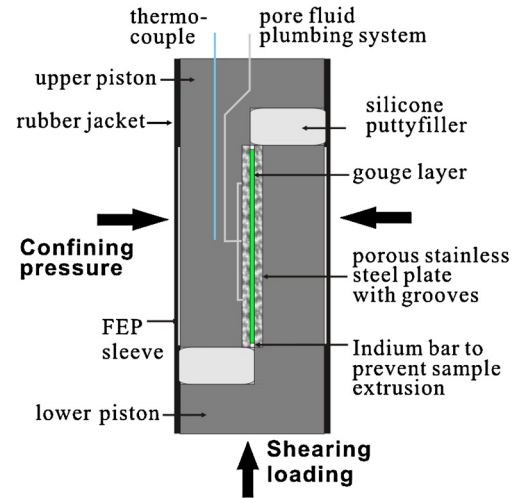


Fig. 2. Sample assembly used for the present direct-shear experiments performed in a triaxial deformation apparatus. See Supplementary material for detailed description.

sequence, and 4) a final velocity stepping sequence. Each velocity stepping sequence (VS-seq) consisted of switching the load-point velocity between 0.1, 1 and 10 $\mu\text{m/s}$. Slide-hold-slide sequences (SHS-seq) consisted of sliding at a constant velocity (1 $\mu\text{m/s}$), arresting the load-point displacement for a systematically varied hold time (t_h), followed by resumption of load-point displacement at the pre-hold velocity. For the wet experiments at 80°C , we also investigated different re-shearing velocities ($V_{SHS} = 0.1, 1$ and $10 \mu\text{m/s}$, Table 1). In each SHS-sequence, we applied 6–9 individual hold events, using hold-times that were progressively increased from 35 s to a maximum of 2.35×10^5 s in roughly three-fold jumps. The sliding displacements imposed after each hold were 0.18–0.5 mm. One control run was performed on a wet sample at 80°C , implementing three VS-sequences separated first by a single 9-h and then by a single 4-h hold-period, and employing a V_{SHS} of 1 $\mu\text{m/s}$. This was done for purposes of comparison with the multi-hold SHS experiments. After testing, representative samples were sectioned and polished, and the microstructure investigated using scanning electron microscopy (SEM).

In each experiment, we determined the apparent frictional strength (μ) as a function of displacement from the ratio of the shear stress supported by the sample layer divided by σ_n . The measured axial displacement was corrected for elastic machine distortion. Using the data obtained in the VS-sequences, the (near) steady-state strength (μ_{ss}) reached before and after each velocity (V) step was employed to determine the friction rate parameter,

Table 1

List of experiments, conditions and key data.

Experiment	Type	T	P_c	P_f	V_{SHS}	W_f	ΔW	Sample behavior			
								VS-seq1	SHS-seq	VS-seq2	β_w
Run-14	dry	20	50	atm.	1	0.83	0.17	s	type 1a	s	0.0086
Run-19	dry	80	50	atm.	1	0.85	0.15	n or w	type 1a	n or w	0.0073
Run-20	dry	140	50	atm.	1	0.88	0.12	w	type 1a	w	0.0060
Run-12	wet	20	65	15	1	0.75	0.25	s	type 1a	s	0.0117
Run-8	wet	80	65	15	0.1	0.65	0.35	w or n	type 2	s	0.0126
Run-6	wet	80	65	15	1	0.70	0.30	w or n	type 2	s	0.0135
Run-4	wet	80	65	15	10	0.78	0.22	w	type 2	s	0.0196
Run-22	wet	140	65	15	1	0.70	0.30	w	type 2	cs	0.0090
Control run	wet	80	65	15	1	0.66	0.33	w	type 2	s	–

Notation: T ($^\circ\text{C}$) = temperature; P_c (MPa) = confining pressure; P_f (MPa) = pore pressure; V_{SHS} ($\mu\text{m/s}$) = re-shearing velocity during SHS-sequence; W_f (mm) = final thickness of the gouge layer; ΔW (mm) = final thickness change of the gouge layer with respect to an initial thickness of 1 mm (± 0.05 mm); β_w (/decade) = frictional healing rate calculated as $d(\Delta\mu_w)/d \log(t_h)$. The abbreviations “s”, “n”, and “w” represent velocity-strengthening, velocity-neutral and velocity-weakening, respectively, while “cs” denotes conditionally velocity-strengthening behavior, which occurred in the VS-seq2 of Run-22 (see Fig. 4 for details). Types 1a and 2 healing behavior occurring during SHS testing are defined as in Fig. 1 and in the text. The single wet control run appearing last in the list was performed with three velocity stepping sequences separated by two SHS events using a single 9-h and a single 4-h hold period.

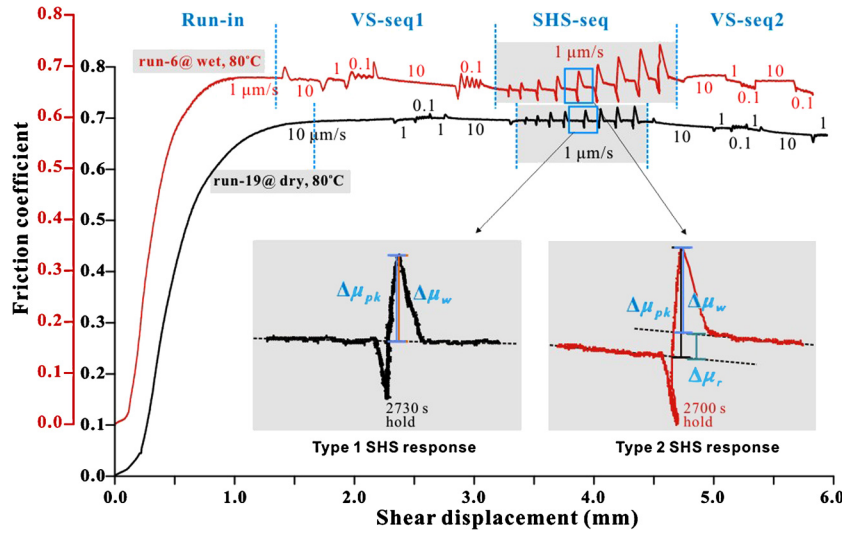


Fig. 3. Typical friction versus displacement data obtained in the present shearing experiments conducted on dry and wet samples. The data shown here were obtained at a temperature of 80 °C and an effective normal stress of 50 MPa. The wet experiment was performed under a confining pressure of 65 MPa and a pore pressure of 15 MPa. Each experiment consisted of 1) a “run-in” at constant velocity, 2) a velocity stepping sequence (VS-seq1), 3) a slide-hold-slide sequence (SHS-seq), and 4) a second velocity stepping sequence (VS-seq2). The inserts illustrate typical data obtained in individual SHS events. Note how changes in steady-state friction coefficient were obtained from data showing slip-weakening (right hand inset, see Supplementary material for details).

$(a - b) = \Delta\mu_{ss}/\Delta\ln V$ (Dieterich, 1979). Positive values of $(a - b)$ indicate stable velocity-strengthening, while negative values indicate potentially unstable velocity-weakening (Marone, 1998a). For the SHS-sequences, we determined the frictional healing parameters ($\Delta\mu_{pk}$, $\Delta\mu_w$ and $\Delta\mu_r$) using the definitions given in Section 2 (see Figs. 1 and 3 inset). See Supplement for details of procedure and data treatment.

4. Results and data analysis

4.1. Friction coefficient versus displacement data

All experiments performed are listed in Table 1. Typical friction versus displacement curves obtained for dry and wet experiments are illustrated in Fig. 3, in this case for tests run at 80 °C. All samples showed quasi steady-state frictional strength in the range 0.63–0.7, regardless of temperature and sliding velocity. In the dry experiment displayed in Fig. 3, the VS-sequences executed both before and after the SHS-seq displayed velocity neutral or slightly velocity-weakening behavior. In the SHS-sequence, each SHS event showed mechanical behavior consistent with Type 1a or 1b frictional healing behavior, i.e. the steady-state friction coefficient remained unchanged ($\Delta\mu_{pk} = \Delta\mu_w$) after each hold period. By contrast, the healing behavior seen in the wet experiment represented in Fig. 3 was characterized by a progressive increase in the quasi steady-state friction level attained after each hold, whereby $\Delta\mu_{pk} > \Delta\mu_w$ and $\Delta\mu_r > 0$ (Type 2 healing). Measured relative to background trends in slip-weakening, these increases persisted throughout each sliding stage of the SHS tests on the wet samples (0.18–0.5 mm). In the wet control experiment that we performed using long hold periods only (Table 1), the increase ($\Delta\mu_r > 0$) persisted for a total displacement of ~ 1.7 mm.

Alongside the above non-Dieterich-type healing behavior observed during the SHS-seq in the wet experiments depicted in Fig. 3, of particular interest is that a switch occurred in the velocity dependence of frictional strength before and after the SHS-seq. The first velocity stepping sequence (VS-seq1) showed minor velocity-weakening behavior, while velocity stepping after the SHS-sequence (VS-seq2) became more stable, generally switching to velocity-strengthening (Fig. 3). This switch did not occur in the dry experiment performed at 80 °C, which showed more or less

velocity neutral behavior after the SHS testing sequence (Fig. 3). Alongside these observations on samples deformed at 80 °C, both dry and wet experiments showed significant effects of temperature on the velocity dependence of friction and on SHS behavior. These effects are addressed below.

4.2. Velocity stepping data

The velocity dependence of friction seen in our experiments is examined further now by comparing the $(a - b)$ values, obtained in the VS-seqs executed before and after the SHS-seq, for all experiments, wet and dry. In both the dry and wet experiments, a transition occurred from velocity-strengthening to velocity-weakening with increasing temperature, as shown in Fig. 4. In the dry experiments, $(a - b)$ values determined before and after the SHS-sequence were indistinguishable, and showed a clear sign-change at ~ 80 °C (Fig. 4a). In the wet experiments, $(a - b)$ values determined before the SHS-sequence were closely similar to those seen in the dry tests, though slightly more scattered, with the transition from velocity-strengthening to velocity-weakening again occurring at 80 °C (Fig. 4b). However, the post-SHS velocity stepping sequences performed on wet samples showed significantly higher $(a - b)$ values, and much wider variability in $(a - b)$, resulting in velocity-weakening being first seen at 140 °C (Fig. 4b). Thus, our results show that, in wet experiments, implementing an interim SHS-seq leads to an increase in $(a - b)$. In most cases (i.e. velocity steps of 1–10 $\mu\text{m/s}$), this resulted in stable velocity-strengthening after the SHS-seq, compared with near neutral or unstable velocity-weakening with stick-slips beforehand, implying that SHS testing had a stabilizing effect on frictional sliding in the wet samples (Table 1), at least within the displacements investigated here.

4.3. Slide-hold-slide results

SHS-seq data from the dry and wet experiments performed at ~ 20 , 80, and 140 °C are shown in Fig. 5a–c. The healing parameters, $\Delta\mu_{pk}$, $\Delta\mu_w$ and $\Delta\mu_r$, were determined from these data for each SHS event, after correction for slip-weakening and occasional slip-strengthening effects (see Supplement). In all experiments, we observed an increase in transient peak strength ($\Delta\mu_{pk}$) with in-

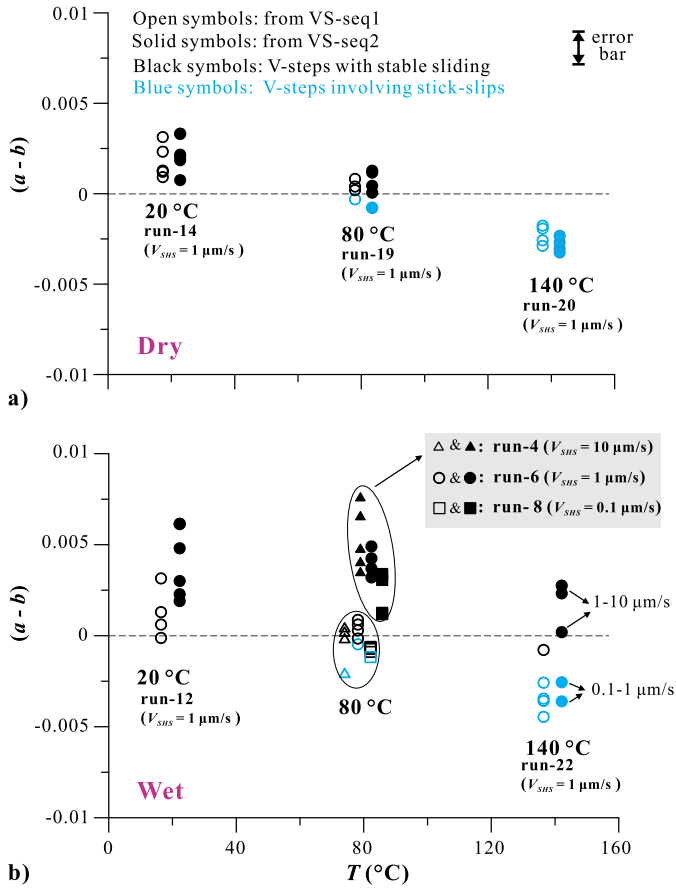


Fig. 4. Temperature (T) dependence of the friction rate parameter ($a - b$), determined in velocity stepping sequences performed before (open symbols, VS-seq1) and after (solid symbols, VS-seq2) SHS testing (SHS-seq) in a) dry and b) wet experiments. Circles, squares and triangles at 80 °C in (b) represent ($a - b$) values obtained in tests employing differing SHS re-shearing velocities (Table 1). Note that the individual sequences of ($a - b$) data obtained at each temperature investigated are plotted at T -values slightly displaced from the corresponding test temperature. This is done for plotting clarity. Some of the ($a - b$) data (blue symbols), were determined at velocities where stick slip occurred. The mean stick-slip friction coefficients were used to determine ($a - b$) in these cases. The VS-seq2 in Run-22 showed stable, velocity-strengthening sliding behavior at velocities stepped between 1 and 10 $\mu\text{m/s}$ (regardless of step direction), but velocity-weakening behavior with stick-slip events at velocities stepped in the range 0.1–1 $\mu\text{m/s}$ (again, regardless of step direction). (For interpretation of the references to color in this figure legend, the reader is referred to the web version of this article.)

creasing hold time and to some extent with increasing temperature. However, the $\Delta\mu_{pk}$ values, and the extent of stress relaxation during hold, measured in dry experiments were lower in magnitude than in the wet experiments (Figs. 3 and 5b), at the same conditions of hold time, temperature and load-point velocity. The post-peak strength or $\Delta\mu_w$ values obtained in both the dry and wet experiments showed the same trends (Fig. 5b–c). As shown in Fig. 5c, $\Delta\mu_{pk}$ and $\Delta\mu_w$ showed a positive dependence on sliding velocity at otherwise similar conditions, i.e. in wet material sheared at 80 °C. In the dry experiments, $\Delta\mu_{pk}$ and $\Delta\mu_w$ were roughly equal in individual SHS events, yielding $\Delta\mu_r \approx$ zero in each case (Type 1a or 1b healing behavior). Positive $\Delta\mu_r$ values (i.e. Type 2 behavior) were seen only in the wet experiments, notably at 80 and 140 °C, where $\Delta\mu_{pk}$ was consistently greater than $\Delta\mu_w$ (Fig. 5b–c). In the wet runs at these temperatures, $\Delta\mu_r$ increased rapidly with hold time, for hold times less than $\sim 60,000$ s, then slowing down to approach an asymptotic saturation value, or even decreasing slightly (Fig. 5b–c). This “saturation effect” was observed in wet samples tested at both 80 and 140 °C, at all V_{SHS} explored, and is illustrated further in Fig. 5d, where the cumula-

tive value of $\Delta\mu_r$ is plotted against cumulative hold time for the wet experiments run at 80 °C, displaying a positive dependence on V_{SHS} . This, along with Fig. 5c, clearly demonstrates the positive dependence of all the three healing parameters on load-point velocity seen in wet samples.

The dependence of the three healing parameters, $\Delta\mu_{pk}$, $\Delta\mu_w$, $\Delta\mu_r$, on (non-cumulative) hold event time for a wet sample deformed at 80 °C is illustrated in the plot of Fig. 5e. The dry result ($\Delta\mu_{pk}$ or $\Delta\mu_w$) at the same temperature is added for comparison. In the dry experiments, the transient peak healing parameter $\Delta\mu_{pk} = \Delta\mu_w$, shows a clear linear relation with $\log(t_h)$ at each temperature investigated, demonstrating Type 1a or classical Dieterich healing (Fig. 1a). The corresponding healing rates (β -values) obtained slightly decrease from 0.0086 to 0.0060/decade, in the temperature range 20–140 °C (Table 1). By contrast, in the wet experiments, $\Delta\mu_{pk}$ exhibits a more complex dependence on t_h . In the wet experiment illustrated in Fig. 5e, $\Delta\mu_{pk}$ gradually increases to a maximum value at $t_h \approx 10^4$ s and then starts to decrease. However, the post-peak frictional weakening ($\Delta\mu_w$) measured for this sample does show a linear relation with respect to $\log(t_h)$. The same general behavior was observed in the data obtained in all wet experiments except that performed at 20 °C (Table 1). The associated β -values for $\Delta\mu_w$ ($\beta_w = d(\Delta\mu_w)/d\log(t_h)$) fall in the range 0.009–0.0196/decade, and exhibit a slight increase with increasing load-point velocity at fixed temperature (Table 1). On this basis, our results for wet samples tested at 80–140 °C can be classified as Type 2 healing and suggest that the direct healing effect ($\Delta\mu_{pk}$) observed in our wet experiments essentially consists of two components, namely a “Dieterich-type” component influencing $\Delta\mu_w$, plus a $\Delta\mu_r$ effect that persists relative to background slip-weakening effects at least for the re-sliding displacements investigated here. In the single wet sample tested at 20 °C, note that $\Delta\mu_r = 0$, corresponding to classical Dieterich-type healing (Fig. 5b).

Fig. 6 displays the friction coefficient versus shear displacement data obtained from the wet control run in which three VS-sequences was separated by two SHS-sequences with single holds of 9 and 4 h. As shown in Fig. 6a, after the first 9-h hold period, the quasi steady-state frictional strength increased markedly, while a smaller increase occurred after the second 4-h hold. Moreover, a transition from velocity-weakening to velocity-strengthening occurred immediately after the 9-h hold period, with velocity-strengthening also persisting after the second 4-h hold.

4.4. Volumetric data and microstructural observations

Our method of measuring sample volume changes during deformation from changes in pore fluid volume, means that we have no volume change data for the dry experiments, except for thickness change data (ΔW) based on direct measurement of sample thickness before and after testing (Table 1). The mean thickness change measured for dry samples was ~ 0.15 mm, corresponding to $\sim 15\%$ porosity reduction, assuming no sample extrusion. Dry samples showed essentially the same microstructure at all temperature investigated (20–140 °C). As illustrated in Fig. 7a–b, boundary shear bands developed at the sample margins with a width varying from 50 to 150 μm . These bands are characterized by marked grain size reduction compared with the bulk of each sample, with most particles in the shear bands being less than 1 μm in diameter. By contrast, the main gouge body seen in the dry samples shows a broad grain size distribution with numerous angular clasts similar in size to the coarsest grains present before deformation (Fig. 7a–c). High magnification imaging of the shear band exhibits a chaotic, granular microstructure similar to the gouge bulk, but with much smaller grain sizes (Fig. 7d).

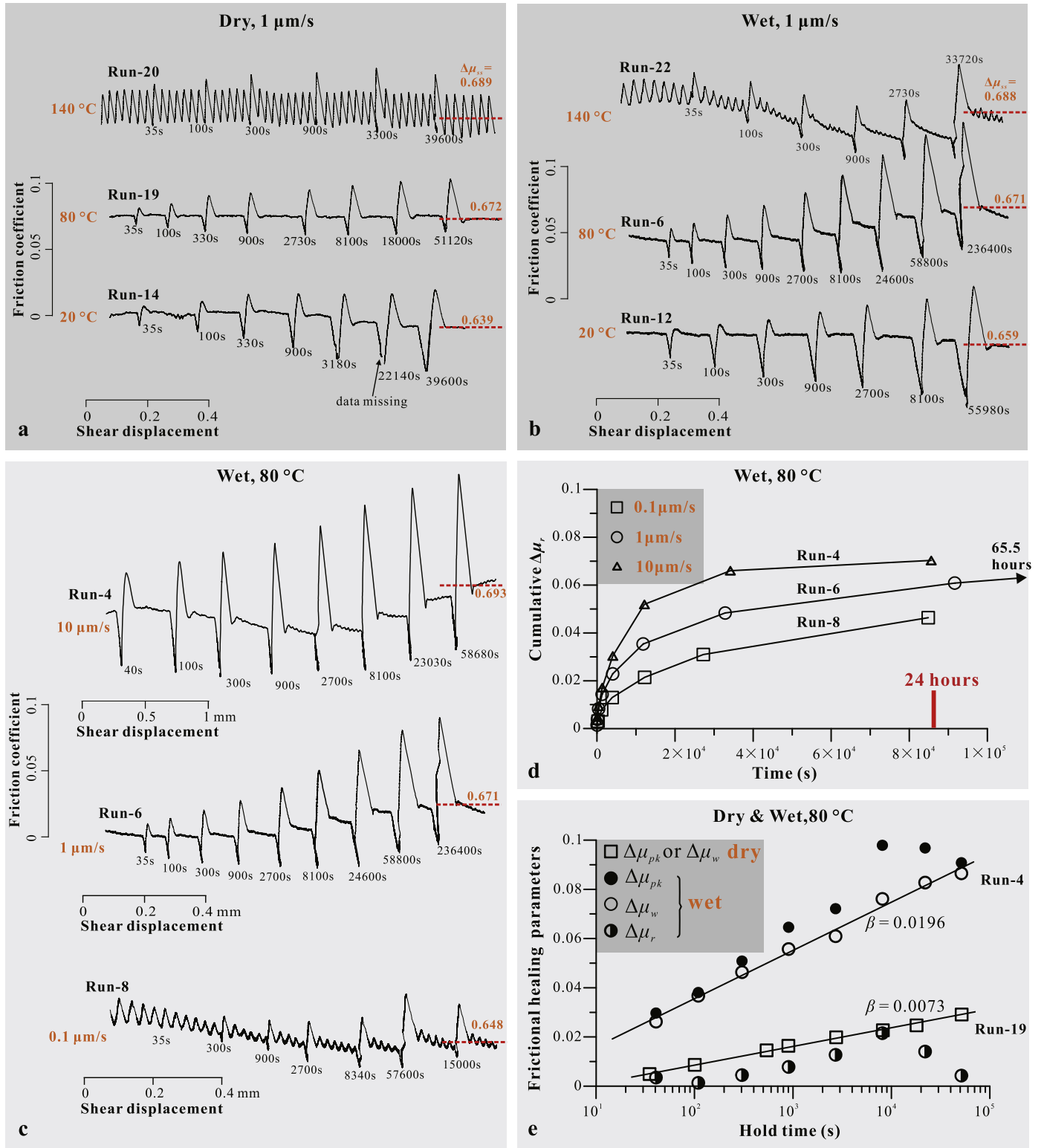


Fig. 5. Representative results obtained in the present SHS test sequences. Hold times indicated in seconds. a) Friction coefficient versus displacement data for dry samples, at 20, 80 and 140 °C, and at a sliding velocity of 1 $\mu\text{m/s}$. b) Same for wet samples. c) Wet tests at 80 °C but conducted at different re-shearing velocities (0.1, 1 and 10 $\mu\text{m/s}$). d) Cumulative, persistent strengthening ($\sum \Delta\mu_r$) as a function of cumulative hold time (denoted as “Time”) with data from runs shown in c). Here, the zero cumulative time point (i.e. zero Time) corresponds to initiation of each SHS testing sequence. e) Frictional healing parameters as a function of the logarithm of hold time per individual hold event, for typical dry and wet experiments at 80 °C. Note that in run-8 (c and d), the last two hold periods were imposed in reverse sequence by accident. In d), the missing long hold time (65.5 h) is indicated with an arrow, to avoid compressing the short time data into an unreadable form.

In the case of the wet experiments, we were able to obtain data on compaction of the gouge layer that occurred during both the VS and SHS testing sequences, as indicated above. Fig. 8a

exhibits a representative result showing dynamic dilatation/compaction of the entire gouge layer in response to a VS-sequence. Regarding the SHS-sequences, significant permanent compaction

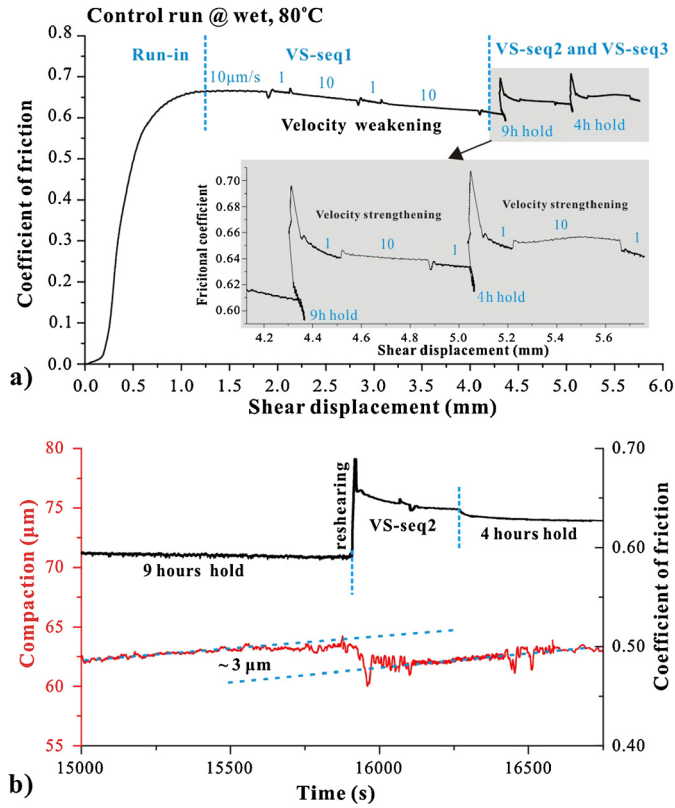


Fig. 6. Results obtained from a control run in which the SHS-sequences were performed for one 9-h and one 4-h hold period only, each separating three velocity stepping sequences (VS-seq1–3). a) Coefficient of friction versus displacement. b) Plot of gouge compaction (pore fluid volume reduction) and friction coefficient versus time, showing dynamic dilatation upon re-shearing after the 9-h hold period.

was recorded, especially during long hold periods, though dynamic dilatation upon re-sliding was not evident (i.e. below the detection limit of $\sim 2 \mu\text{m}$, see Supplement and Fig. 8b). The control experiment featuring two long holds showed large amounts of compaction plus measurable dilatation upon shearing (Fig. 6b). Typical values of ΔW measured for the wet-tested samples lay around a mean of 0.28 mm (0.22–0.35 mm, Table 1), twice that measured for the dry experiments. The deformed wet samples show a similar but more uniform microstructure (Fig. 7e) compared with the dry samples (Fig. 7a–c). Though visible, the shear bands are less distinct and much denser than those seen in the dry samples (cf. Figs. 7f–h versus 7b–d). The bulk gouge in the wet samples is also finer than in the dry, with a lower proportion of coarse clasts (Fig. 7e). High magnification images showed the shear bands consist of rounded, (sub)micrometer-sized grains that are cemented or sintered together (Fig. 7g). These sintered aggregates are locally cut by shear-band-parallel cracks that presumably formed during sample unloading or thin-section preparation (Fig. 7h), suggesting a co-deformational origin of the sintered microstructure.

5. Discussion

5.1. Type 1a or Dieterich-type healing in the dry samples

As described above, the SHS stage of our dry experiments showed conventional Dieterich-type (i.e. Type 1a) healing behavior at all temperatures investigated, this being characterized by a linear relation between $\Delta\mu_{pk}$ and $\log(t_h)$ and by unchanged steady-state friction before and after each SHS event ($\Delta\mu_r = 0$). This behavior is qualitatively identical to that seen

in previous experiments performed on dry quartz and dry granite gouge samples at similar conditions (e.g. Marone, 1998b; Frye and Marone, 2002). The healing rates obtained in our dry experiments (0.0060–0.0086/decade) are also comparable to those seen in dry quartz and granite gouges. Based on the microstructural (Fig. 7) and thickness change data (Table 1) obtained for our dry samples, we infer that cataclastic grain size reduction and grain rearrangement, leading to granular flow focused in the shear bands found at the boundaries of the samples, were the dominant deformation mechanisms operating during active sliding periods. This is consistent with magnitude of measured compaction being relatively small (Table 1). Though we have no direct evidence ourselves, from the conclusions of previous studies addressing DH (Dieterich, 1979), we infer that the mechanisms controlling $\Delta\mu_{pk}$ in our dry SHS testing sequence, likely involved static growth or strengthening of solid–solid contact points, due to contact creep or surface diffusive transport.

5.2. Type 2 (non-Dieterich-type) healing seen in wet samples

The Type 2 or “non-Dieterich-type” healing behavior seen in our wet experiments is a first-time observation for carbonate fault rocks. The associated increase in $(a - b)$, or slip stabilization effect, is also novel. Similar healing behavior, i.e. with $\Delta\mu_r > 0$, has been reported previously but only rarely. Examples include experiments on wet quartz gouge subjected to healing at 65 °C (Yasuhara et al., 2005), and on wet gypsum at room temperature (Muhuri et al., 2003). In line with our observations (Fig. 3), the NDH behavior reported by Yasuhara et al. (2005) occurred only at elevated temperature (65 °C). NDH behavior was also absent in the dry control experiment on gypsum reported by Muhuri et al. (2003). Unfortunately, neither Yasuhara et al. (2005) nor Muhuri et al. (2003) reported or analyzed their healing data in a way that can be easily compared with ours. Nonetheless, taking into account their findings as far as possible, we now consider what mechanisms could have played a role in our wet experiments, and how could these explain the Type 2 (non-Dieterich-type) healing behavior observed.

As in the dry samples, the microstructure of our wet samples shows that active displacement was accommodated by cataclastic grain size reduction and flow, focused in localized boundary shear bands. In addition, the sintered/cemented internal microstructure of these bands in the wet samples suggests the operation of a diffusive mass transfer process, such as pressure solution. Previous 1-D compaction experiments on wet granular calcite have also shown that intergranular pressure solution (IPS) is an important deformation mechanism under the P–T conditions investigated here (X. Zhang et al., 2010). This type of process was inferred to produce enhanced NDH behavior by both Muhuri et al. (2003) and Yasuhara et al. (2005), on the basis of microstructural evidence, such as crack sealing and pore cementation. In addition, many other studies have demonstrated that solution transfer can significantly enhance healing processes in fault gouges sheared under (hydrothermal) conditions where solution transfer is possible (e.g. Olsen et al., 1998; Bos and Spiers, 2002). Frictional re-strengthening in these previous studies was attributed to 1) an increase in intrinsic intergranular cohesive strength (Yasuhara et al., 2005), 2) an increase in cohesive solid–solid contact area within the gouge zone (Niemeijer et al., 2008), or 3) dilatation following fluid-assisted compaction during hold (Bos and Spiers, 2002). Any of these three re-strengthening processes could potentially contribute to the transient peak healing effect ($\Delta\mu_{pk}$) seen in our wet experiments at 80–140 °C, presumably through their operation within the boundary shear band, and/or the sample body. However, the persistent strengthening effect ($\Delta\mu_r$) that we observe is not explained by any of them, as discussed below.

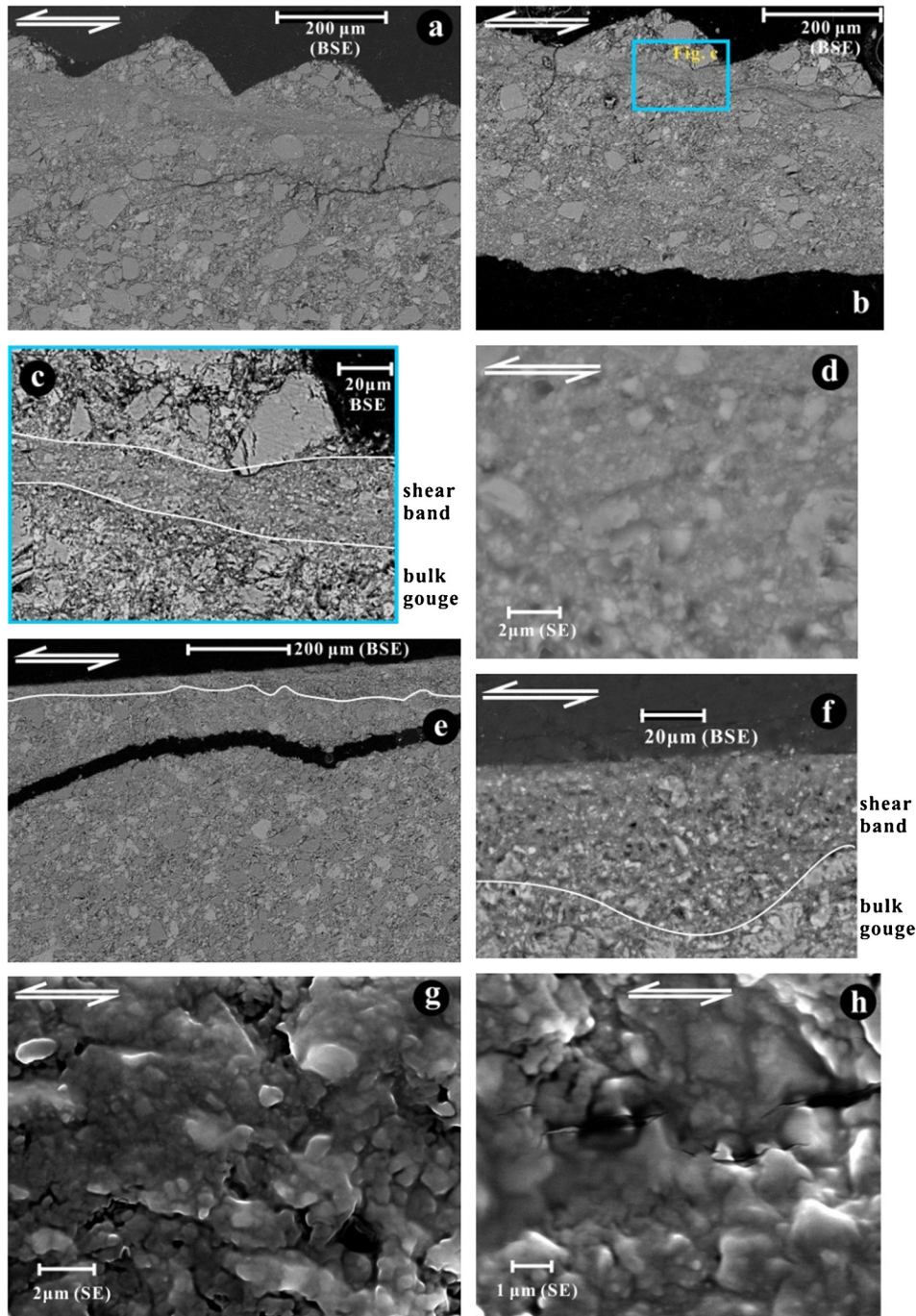


Fig. 7. SEM microstructures of samples tested dry (a–d) and wet (e–h) at 80 °C. Images a, b, c, e and f were obtained using backscattered electrons. Images d, g and h were obtained from boundary shear zones in wet samples using secondary electrons. Shear sense is as indicated. Note the impression of the toothed sample grips in images (a) and (b) and the sintered appearance of the submicrometer-sized grains in (g) and (h). Boundary shear bands are clearly visible in the dry samples (images a–c). They are also visible in the wet samples (e, f), but less clearly, so have been delineated. In (e) and (f), the impressions of the toothed sample grips are not preserved, as the sample surfaces stuck to the grooved piston surface (porous stainless steel, Fig. 2) when dismantled.

First, in the case of intergranular cohesion, an increase in steady-state friction has been proposed to occur when aggregates of welded grains, formed during hold periods, are forced to move as an assemblage upon re-shearing, requiring more mechanical work for dilatation (see Fig. 6 of Yasuhara et al., 2005). Evidence for grain aggregation and cementation can be seen in the shear bands in our wet samples (Fig. 7g–h). However, discrete clusters are not observed. To examine the viability of this mechanism further, we checked the volumetric data obtained in the control run (Fig. 6a), in which a long hold period (9 h) was immediately initiated after the first VS-seq, yielding large transient ($\Delta\mu_{pk}$) and quasi steady-

state ($\Delta\mu_r$) healing effects. Transient dilation upon re-shearing after this hold was around 4.5 μm settling back to a longer lived baseline effect of $\sim 3 \mu\text{m}$ (Fig. 6b). The transient healing effect (i.e. $\Delta\mu_{pk}$) may be explainable by the transient dilatation, perhaps reflecting an effect of the type envisaged by Yasuhara et al. (2005). However, the baseline volume increase cannot have been important in determining $\Delta\mu_r$, i.e. in producing the Type 2 healing behavior in our wet experiments at elevated temperatures, because active dilatation was not measured during the steady sliding stages of the experiments. Instead, the samples compacted continuously (see Fig. 8b).

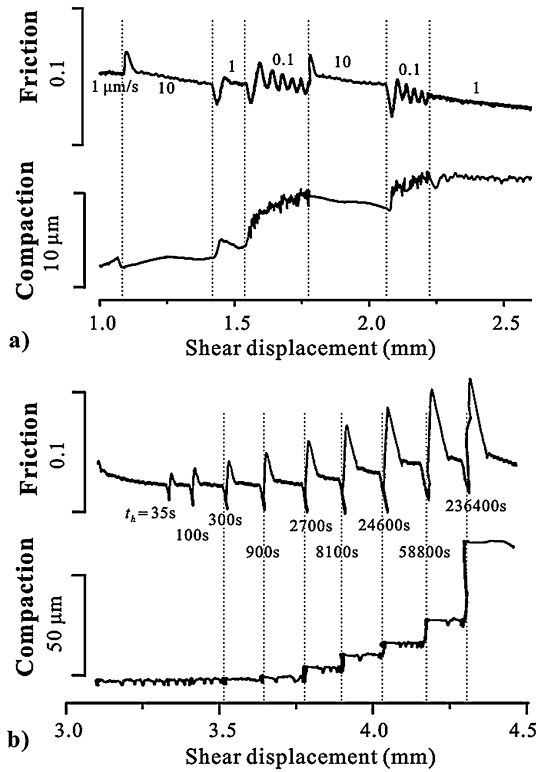


Fig. 8. Plot of friction coefficient and gouge compaction versus displacement, for the a) VS-seq1 and b) SHS testing sequences performed on a wet sample tested at 80 °C (Run-6). The compaction data was obtained from pore fluid volume changes measured at constant fluid pressure.

Static increase in grain contact cohesion or static growth in grain contact area, due to fluid-enhanced indentation creep (IPS), neck growth (Hickman and Evans, 1992) or hydrolytic weakening effects (Frye and Marone, 2002), without any clustering or other microstructural change occurring during hold or re-shearing (as envisaged by Niemeijer et al., 2008), is also unlikely to be the reason for the positive values of $\Delta\mu_r$, hence Type 2 behavior, seen in our wet tests. This is because the enlarged or strengthened contacts would be immediately destroyed when re-shearing the gouge layer. Similar reasoning also makes IPS-enhanced compaction, followed by dilatation of pores between individual grains (Bos and Spiers, 2002), an unlikely explanation, as the strength contribution associated with dilation and increased dilation angle falls to zero as the steady-state sliding porosity (or bulk background compaction) is re-established during re-shear. As a result of this, compaction/dilatation can again only contribute to transient peak healing ($\Delta\mu_{pk}$).

Here we propose that the increased dynamic friction ($\Delta\mu_r$) observed in the SHS-sequences of our wet experiments at 80–140 °C is due to more complex, permanent effects of porosity reduction, occurring in both the shear bands and the gouge body. Our argument is as follows. First, marked compaction was detected during the hold periods by the precision volumetric pump employed for pore pressure control in the wet tests (Fig. 8b). This compaction reflects the sum of the sample pore volume change occurring in both the shear band and bulk gouge (Chambon et al., 2006). Second, porosity reduction by IPS is indicated by the fact that, though both the wet and dry samples had the same initial thickness (1 ± 0.05 mm), the final thickness was much less in the wet samples (~ 0.72 mm) than in the dry samples (~ 0.85 mm). In line with previous evidence for pressure solution in calcite under the present conditions (X. Zhang et al., 2010), this implies that compaction and porosity reduction by pressure solution must have occurred during

the hold periods of our SHS runs, causing an increase in grain-to-grain contact area, contact strength and dilation angle, in both the gouge bulk and boundary shears. The much larger shear stress relaxation that occurred during the hold periods of our wet experiments compared with the dry ones (Figs. 3 and 5a–b) further supports such a process (Marone and Saffer, 2015). We infer that the associated microstructural changes produced a transient increase in frictional strength of the samples that led to the observed peak strength on re-shearing ($\Delta\mu_{pk}$ effect), as interpreted in many previous studies (e.g. Yasuhara et al., 2005). During on-going re-shearing, however, the pre-hold porosity and microstructure were clearly not (fully) restored, as in classical Dieterich healing. Instead, the residual healing effect ($\Delta\mu_r$), seen in our wet samples sheared at 80–140 °C, implies that re-shearing was accommodated, presumably in a boundary shear, in gouge material having persistently lower porosity and/or higher contact cohesion, hence persistently higher strength, than the active gouge zone prior to hold.

To achieve such persistent changes in slip zone strength ($\Delta\mu_r$) during post-hold re-shearing, two possible changes in microstructure can be envisaged. One possibility is permanent widening of the principal boundary shear band upon re-shearing (or formation of a new, wider shear band). This would lead to lower shear band strain rates at a given imposed velocity, and hence to more effective internal competition of compaction, by IPS, versus dilatation associated with cataclastic/granular shear flow (Niemeijer and Spiers, 2007). The result would be lower steady-state porosity and higher strength. This type of strengthening effect is similar to that envisaged in the model by Sleep et al. (2000). However, on obvious changes in shear band thickness were observed in our experiments, compared with runs conducted on calcite by Verberne et al. (2013b) without a SHS-sequence. A second possibility is grain size reduction (i.e. grain breakage) occurring within the principal boundary shear upon post-hold re-shearing. This too would lead to an enhancement of compaction by pressure solution relative to dilatation by cataclastic/granular flow, since the rate of pressure solution compaction increases with decreasing grain size (X. Zhang et al., 2010). We favor this explanation because of the extreme narrowness and submicron grain size of the boundary shear bands seen in our samples (Fig. 7e–h). Nonetheless, previous microphysical models, based on gouge deformation by granular flow plus pressure solution, predict increasing steady-state friction with both decreasing particle size and with increasing shear band thickness (Niemeijer and Spiers, 2007; Den Hartog and Spiers, 2014), so that either explanation seems viable. A quantitative model explaining both the steady-state and transient frictional and healing behavior observed in this study, including persistent strengthening, will be developed in a future paper.

Having identified possible origins for $\Delta\mu_r$, and again noting the modest dilation occurring upon re-shear (Fig. 8b), we propose that the remaining part of the direct healing effect ($\Delta\mu_{pk}$) observed in our wet experiments, i.e. $\Delta\mu_w = \Delta\mu_{pk} - \Delta\mu_r$, reflects changes in contact area and porosity, resulting from reversible static contact growth and/or strengthening, as envisaged in the classical Dieterich model for healing. This is supported by the logarithmic, Dieterich-type dependence of hold time exhibited by $\Delta\mu_w$ in our data (Fig. 5e). Hence, our interpretation of $\Delta\mu_{pk}$ in our experiments is that it consists of a Dieterich-type part ($\Delta\mu_w$) related to reversible contact growth and strengthening, plus a non-Dieterich-type part ($\Delta\mu_r$) related to pressure solution compaction with a concomitant increase in contact area, all enhanced by permanent grain size reduction and/or shear band broadening. Similar healing partitioning was previously proposed by Frye and Marone (2002) to explain the enhanced healing observed in quartz gouge sheared at relatively high relative humidities at room temperature.

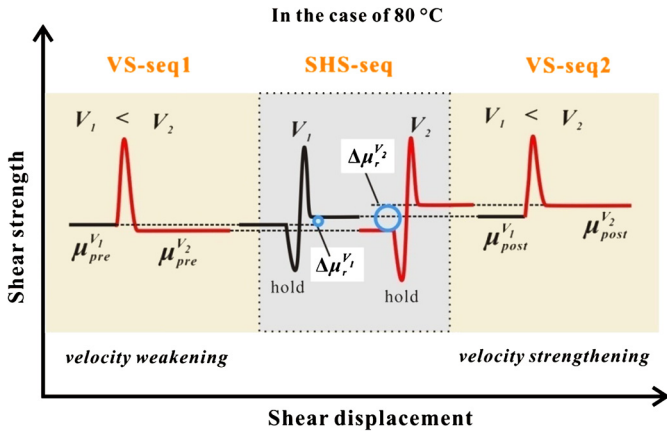


Fig. 9. Schematic diagram illustrating how “interseismic” healing may cause slip “stabilization”, i.e. an increase in $(a - b)$, in the present experiments at hydrothermal conditions (e.g. 80 °C). In line with the “VS-SHS-VS” sequences implemented in our experiments, we infer the following. 1) VS-seq1: the pre-healing steady-state friction coefficients are $\mu_{pre}^{V_1}$ and $\mu_{pre}^{V_2}$ for sliding velocities of V_1 and V_2 ($V_1 < V_2$); 2) SHS-seq: the “interseismic” hold period causes residual, persistent strengthening ($\Delta\mu_r$), which accumulates in repeated healing (SHS) cycles and depends positively on active sliding velocity (Fig. 5d), such that $\sum \Delta\mu_r^{V_1} < \sum \Delta\mu_r^{V_2}$; 3) VS-seq2: the post-healing steady-state friction coefficients here are $\mu_{post}^{V_1} = \mu_{pre}^{V_1} + \sum \Delta\mu_r^{V_1}$ and $\mu_{post}^{V_2} = \mu_{pre}^{V_2} + \sum \Delta\mu_r^{V_2}$. Note that the SHS-seq presented includes one SHS event for each of the two sliding velocities represented. The change in $(a - b)$ after versus before healing (i.e. SHS testing) can thus be determined from the difference in the accumulated persistent strengthening ($\sum \Delta\mu_r$) for different velocities, that is from $\Delta(a - b) = (\sum \Delta\mu_r^{V_2} - \sum \Delta\mu_r^{V_1}) / (\ln V_2 - \ln V_1)$. This scenario applies to the results obtained at 80 and 140 °C, but the behavior seen at 140 °C is more complex due to oscillatory stick-slips.

5.3. Slip stabilization and its cause

In our wet experiments, we observed a clear increase in $(a - b)$ after the SHS-sequence (Fig. 4). This “fault stabilization” effect was totally absent in dry samples. Previous studies report a similar transition from unstable stick-slip to stable sliding, but this was caused by continued wear with accumulated displacement, especially for slip on initially bare surfaces (e.g., Tullis and Weeks, 1986; Wong and Zhao, 1990). By contrast, almost all previous experiments on simulated fault gouges show the opposite trend, i.e. from velocity-strengthening to velocity-weakening with increasing shear displacement (Dieterich, 1979; Marone et al., 1990; Beeler et al., 1996; Richardson and Marone, 1999). In our experiments, the stabilization effect was only seen in the wet experiments after the SHS stage, so is unlikely to be due to accumulated displacement. This is confirmed by the control run in which we imposed a 9-h hold, whereby stabilization occurred immediately after (Fig. 6a).

We note here that the stabilization effect seen in our wet experiments at elevated temperatures was always accompanied by Type 2 (NDH) behavior, characterized by a permanent increase ($\Delta\mu_r$) in quasi steady-state friction. As shown in Fig. 5c–d, the magnitude of $\Delta\mu_r$ obtained in the SHS-sequences increases with increasing load-point velocity. With reference to Fig. 9, the increase in $(a - b)$ following SHS testing can accordingly be explained by the difference in the accumulated, persistent strengthening ($\sum \Delta\mu_r^{V_1}$ and $\sum \Delta\mu_r^{V_2}$) measured at velocities V_1 and V_2 . The change in $(a - b)$ can be determined: $\Delta(a - b) = (\sum \Delta\mu_r^{V_2} - \sum \Delta\mu_r^{V_1}) / (\ln V_2 - \ln V_1)$. Based on the data given in Fig. 5d, $\Delta(a - b)$ in our wet samples are ~ 0.0043 for velocity steps of 1–10 $\mu\text{m/s}$, and ~ 0.048 for velocity steps of 0.1–1 $\mu\text{m/s}$. These values are consistent with the increase in $(a - b)$ obtained from the VS-sequences performed before and after SHS testing (i.e. with the vertical offset of the VS-seq2 data with respect to VS-seq1 in Fig. 4b), suggesting that the stabilization effect may be due to the

persistent strengthening effect ($\Delta\mu_r$) discussed above. However, this does not explain the effect seen at 20 °C, where $\Delta\mu_r$ is more or less zero. Further work is needed to resolve this issue.

5.4. Implications

Our SHS observations indicate that standard concepts of frictional healing, as embodied in the log-linear healing effect incorporated in the classic RSF formulation (Dieterich, 1979) (i.e. Type 1a healing), need to be modified to describe the interseismic re-strengthening ($\Delta\mu_{pk}$ and $\Delta\mu_r$ behavior) of carbonate-rich fault gouges under hydrothermal conditions where chemically enhanced healing processes such as pressure solution are active. For the same reasons, our results imply that previous estimates of frictional healing rates in simulated quartz gouges, based on the log-linear fits to dry and room temperature healing data (e.g. Marone, 1998b), may significantly underestimate hydrothermal healing rates and magnitudes ($\Delta\mu_{pk}$) that actually apply to the (much longer) interseismic periods of natural faults. It is therefore important to take into account the effects of in-situ conditions and of fluid–rock interaction processes when extrapolating the lab-derived healing rates to natural faults (cf. Nakatani and Scholz, 2004). In addition, slip associated with aftershocks and changes in fault loading rate may also have important effects on fault re-strengthening processes in nature, which need to be taken into account (Fig. 7c, Marone and Saffer, 2015).

Our results for carbonate gouge indicate that the “non-Dieterich-type” (Type 2) healing observed under wet conditions can cause an increase in $(a - b)$ value. If these results apply to natural faults in carbonates, the implication is that repeated operation of interseismic healing processes, under otherwise unchanging conditions, may tend to stabilize rupture nucleation, assuming that the elastic stiffness of the surrounding rock does not decrease with respect to the critical stiffness for unstable (stick-)slip (Scholz, 2002). Other factors that can affect rupture nucleation, in nature, of course include changes in the tectonically-driven loading rate (Wong and Zhao, 1990) and in the magnitude of local stress perturbations (Scholz, 2002).

At the same time, our data for wet samples show that $(a - b)$ decreases with increasing temperature (Fig. 4b), transitioning from velocity-strengthening to velocity-weakening with increasing temperature, hence depth. If our results on the effect of persistent strengthening on $(a - b)$ apply to natural faults, this in turn suggests that the stabilization effect of persistent strengthening occurring during interseismic healing could result in the upper limit of the seismogenic zone migrating to deeper crustal levels in carbonate terrains (Fig. 4b). In principle, this effect, combined with the enhanced frictional healing effect will tend to promote the occurrence of earthquakes with progressively increasing magnitude in an increasingly narrow depth range. We note, however, that we could find no evidence to support the existence of such effects from natural earthquake records. The absence of such evidence may, of course, reflect effects of normal stresses or temperatures not accessed in our tests, or the operation of other processes, such as the initiation or activation of a new, weaker fault plane or principal slip zone at similar crustal level (Collettini et al., 2014), rather than reactivation of a healed one.

Additional factors that may complicate the evolution of seismicity and the seismic cycle in carbonate terrains include the rapid temperature increase caused by nucleation or propagation of an earthquake rupture (e.g. De Paola et al., 2011). Such heating may cause unstable slip at shallower depths than otherwise expected in the velocity-strengthening regime (i.e. where normally $T < 80$ °C). Moreover, subsequent temperature decay with time along with the healing effects ($\Delta\mu_r$) seen in our data, could have important effects on the evolution of $(a - b)$ and hence on aftershock nucleation

and distribution with depth (Chiarabba et al., 2009). Studies of 4-D seismological data obtained for earthquakes occurring in carbonate terrains, such as the Apennines, may offer a means of assessing these speculations in future.

6. Conclusions

In the present study, we have investigated the frictional stability and healing behavior of a simulated carbonate fault gouge under dry and wet conditions, at temperatures in the range 20–140 °C and σ_n of 50 MPa. The following conclusions have been drawn.

- 1) Velocity stepping tests yielded quasi steady-state friction coefficients in the range 0.63–0.7, depending on sliding velocity and temperature, in agreement with previous data for wet and dry carbonate gouges. However, SHS testing under hydrothermal conditions showed non-Dieterich-type healing behavior, characterized by a persistent increase in quasi steady-state friction coefficient after hold, superimposed on any background slip-weakening or slip-strengthening trends. This behavior was not seen in dry experiments.
- 2) Our experiments on wet carbonate gouge are the first to show that slide-hold-slide testing, or interseismic healing, can cause changes in slip stability, i.e. an increase in the RSF rate parameter ($a - b$). In our experiments, this increase leads to a concomitant shift in the temperature above which velocity-weakening becomes important in wet calcite-rich gouge from around 80 °C to above 140 °C.
- 3) This persistent strengthening observed in our experiments is inferred to reflect the frictional behavior of localized principal shear bands, and to be related to enhanced compaction of these bands by internal pressure solution, due to permanent grain size reduction and/or to shear band broadening upon re-shear.
- 4) If the stabilization effect applies to faults in tectonically active carbonate terrains, it implies a tendency for shift in the upper limit of the seismogenic zone to deeper, warmer crustal levels, following interseismic healing events. This shift will tend to promote the occurrence of progressively stronger earthquakes at deeper levels in a gradually shrinking seismogenic zone. In practice, competing processes, such as the initiation of new (weaker) faults will likely complicate the above picture. Future studies of seismicity in carbonate terrains may shed light on whether the effects observed in our experiments do actually play any role in nature.

Acknowledgements

We would like to thank P. van Krieken and G. Kastelein for their technical support in maintaining the testing machine. We thank C. Marone, B. Carpenter and an anonymous reviewer for their reviews of this paper. JC was funded by State Key Laboratory of Earthquake Dynamics (LED2010A03) and the Netherlands Center for Solid Earth Science (ISES) grant 2013-103, while BAV was supported by ISES grant 2011-75.

Appendix A. Supplementary material

Supplementary material related to this article can be found online at <http://dx.doi.org/10.1016/j.epsl.2015.03.044>.

References

- Beeler, N.M., Tullis, T.E., Weeks, J.D., 1996. Frictional behavior of large displacement experimental faults. *J. Geophys. Res.* 101, 8697–8715.
- Bernard, J.E., Hubert, W., Diraison, M., 2006. Seismicity wedge beneath the Upper Rhine Graben due to backwards Alpine push? *Tectonophysics* 428, 49–64.
- Blanpied, M.L., Lockner, D.A., Byerlee, J.D., 1995. Frictional slip of granite at hydrothermal conditions. *J. Geophys. Res.* 100, 13045–13064.
- Bos, B., Spiers, C.J., 2002. Fluid-assisted healing processes in gouge bearing faults: insights from experiments on a rock analogue system. *Pure Appl. Geophys.* 159, 2537–2566.
- Carpenter, B.M., Marone, C., Saffer, D.M., 2011. Weakness of the San Andreas Fault revealed by samples from the active fault zone. *Nat. Geosci.* 4, 251–254. <http://dx.doi.org/10.1038/ngeo1089>.
- Carpenter, B.M., Scuderi, M.M., Collettini, C., Marone, C., 2014. Frictional heterogeneities on carbonate-bearing normal faults: insights from the Monte Maggio Fault, Italy. *J. Geophys. Res. Solid Earth* 119. <http://dx.doi.org/10.1002/2014JB011337>.
- Chambon, G., Schmittbuhl, J., Corffdir, A., 2006. Frictional response of a thick gouge sample: 1. Mechanical measurements and microstructures. *J. Geophys. Res.* 111, B09308. <http://dx.doi.org/10.1029/2003JB002731>.
- Chen, J., Yang, X., Ma, S., Spiers, C.J., 2013. Mass removal and clay mineral dehydration/rehydration in carbonate-rich surface exposures of the 2008 Wenchuan Earthquake fault: geochemical evidence and implications for fault zone evolution and coseismic slip. *J. Geophys. Res.* 118, 474–496.
- Chiarabba, C., Amato, A., Anselmi, M., et al., 2009. The 2009 L'Aquila (central Italy) MW6.3 earthquake: main shock and aftershocks. *Geophys. Res. Lett.* 36 (18), 1–6.
- Collettini, C., Carpenter, B.M., Viti, C., et al., 2014. Fault structure and slip localization in carbonate-bearing normal faults: an example from the northern Apennines of Italy. *J. Struct. Geol.* 67, 154–166.
- Coulomb, C.A., 1785. Théorie des machines simples. *Mém. Math. Phys. Acad. Sci.* 10, 161–331.
- Den Hartog, S., Spiers, C.J., 2014. A microphysical model for fault gouge friction applied to subduction megathrusts. *J. Geophys. Res.* 119, 1510–1529. <http://dx.doi.org/10.1002/2013JB010580>.
- De Paola, N., Hirose, T., Mitchell, T., 2011. Fault lubrication and earthquake propagation in thermally unstable rocks. *Geology* 39 (1), 35–38.
- Dieterich, J.H., 1979. Modeling of rock friction: 1. Experimental results and constitutive equations. *J. Geophys. Res.* 84, 2161–2168.
- Frye, K.M., Marone, C., 2002. Effect of humidity on granular friction at room temperature. *J. Geophys. Res.* 107 (B11), 2309. <http://dx.doi.org/10.1029/2001JB000654>.
- Han, R., Shimamoto, T., Hirose, T., Ree, J., Ando, J., 2007. Ultralow friction of carbonate faults caused by thermal decomposition. *Science* 316, 878–881.
- He, C., Wang, Z., Yao, W., 2007. Frictional sliding of gabbro gouge under hydrothermal conditions. *Tectonophysics* 445, 353–362.
- Hickman, S.H., Evans, B., 1992. Growth of grain contacts in halite by solution-transfer: implications for diagenesis, lithification, and strength recovery. In: Evans, B., Wong, T.-F. (Eds.), *Fault Mechanics and Transport Properties of Rocks*. Elsevier, New York, pp. 253–280.
- Karner, S.L., Marone, C., Evans, B., 1997. Laboratory study of fault healing and lithification in simulated fault gouge under hydrothermal conditions. *Tectonophysics* 277, 41–55.
- Li, Y.-G., Vidale, J.E., Day, S.M., Oglesby, D.D., Cochran, E., 2003. Postseismic fault healing on the rupture zone of the 1999 M 7.1 Hector Mine, California, earthquake. *Bull. Seismol. Soc. Am.* 93, 854–869.
- Marone, C., Vidale, J.E., Ellsworth, W., 1995. Fault healing inferred from time dependent variations in source properties of repeating earthquakes. *Geophys. Res. Lett.* 22, 3095–3098.
- Marone, C., 1998a. Laboratory-derived friction laws and their application to seismic faulting. *Annu. Rev. Earth Planet. Sci.* 26, 643–696. <http://dx.doi.org/10.1146/annurev.earth.26.1.643>.
- Marone, C., 1998b. The effect of loading rate on static friction and the rate of fault healing during the earthquake cycle. *Nature* 391, 69–72.
- Marone, C., Saffer, D.M., 2015. The mechanics of frictional healing and slip instability during the seismic cycle. In: Kanamori, H., et al. (Eds.), *Treatise on Geophysics*, 2nd edition. Elsevier, Oxford, UK, 45 pp.
- Marone, C., Raleigh, C.B., Scholz, C.H., 1990. Frictional behavior and constitutive modeling of simulated fault gouge. *J. Geophys. Res.* 95, 7007–7025.
- Mirabella, F., Barchi, M., Lupattelli, A., Stucchi, E., Ciaccio, M.G., 2008. Insights on the seismogenic layer thickness from the upper crust structure of the Umbria-Marche Apennines (central Italy). *Tectonics* 27, TC1010. <http://dx.doi.org/10.1029/2007TC002134>.
- Muhuri, S.K., Dewers, T.A., Scott Jr., T.E., Reches, Z., 2003. Interseismic fault strengthening and earthquake-slip instability: friction or cohesion? *Geology* 31, 881–884. <http://dx.doi.org/10.1130/G19601.1>.
- Nakatani, M., Mochizuki, H., 1996. Effects of shear stress applied to surfaces in stationary contact on rock friction. *Geophys. Res. Lett.* 23, 869–872.
- Nakatani, M., Scholz, C.H., 2004. Frictional healing of quartz gouge under hydrothermal conditions: 1. Experimental evidence for solution transfer healing mechanism. *J. Geophys. Res.* 109, B07201. <http://dx.doi.org/10.1029/2001JB001522>.
- Niemeijer, A.R., Spiers, C.J., 2007. A microphysical model for strong velocity weakening in phyllosilicate-bearing fault gouges. *J. Geophys. Res.* 112, B10405. <http://dx.doi.org/10.1029/2007JB005008>.

- Niemeijer, A., Marone, C., Elsworth, D., 2008. Healing of simulated fault gouges aided by pressure solution: results from rock analogue experiments. *J. Geophys. Res.* 113, B04204. <http://dx.doi.org/10.1029/2007JB005376>.
- Olsen, M.P., Scholz, C.H., Léger, A., 1998. Healing and sealing of a simulated fault gouge under hydrothermal conditions: implications for fault healing. *J. Geophys. Res.* 103, 7421–7430.
- Richardson, E., Marone, C., 1999. Effects of normal stress vibrations on frictional healing. *J. Geophys. Res.* 104 (B12), 28,859–28,878.
- Ruina, A., 1983. Slip instability and state variable friction laws. *J. Geophys. Res.* 88, 10359–10370.
- Scholz, C.H., 2002. *The Mechanics of Earthquakes and Faulting*, 2nd edition. Cambridge Univ. Press, Cambridge, New York, 471 pp.
- Scuderi, M.M., Niemeijer, A.R., Collettini, C., Marone, C., 2013. Frictional properties and slip stability of active faults within carbonate–evaporate sequences: the role of dolomite and anhydrite. *Earth Planet. Sci. Lett.* 369–370, 220–232.
- Sibson, R.H., 1982. Fault zone models, heat flow, and the depth distribution of earthquakes in the continental crust of the United States. *Bull. Seismol. Soc. Am.* 72 (1), 151–163.
- Sleep, N.H., Richardson, E., Marone, C., 2000. Physics of strain localization in synthetic fault gouge. *J. Geophys. Res.* 105 (B11), 25,875–25,890.
- Tenthorey, E., Cox, S.F., 2006. Cohesive strengthening of fault zones during the interseismic period: an experimental study. *J. Geophys. Res.* 111, B09202. <http://dx.doi.org/10.1029/2005JB004122>.
- Tullis, T.E., Weeks, J.D., 1986. Constitutive behavior and stability of frictional sliding of granite. *Pure Appl. Geophys.* 124, 383–414.
- Verberne, B.A., He, C., Spiers, C.J., 2010. Frictional properties of sedimentary rocks and natural fault gouge from the Longmenshan Fault Zone, Sichuan, China. *Bull. Seismol. Soc. Am.* 100, 2767–2790.
- Verberne, B.A., De Bresser, J.H.P., Niemeijer, A.R., Spiers, C.J., De Winter, D.A.M., Plümpner, O., 2013a. Nanocrystalline slip zones in calcite fault gouge show intense crystallographic preferred orientation: crystal plasticity at subseismic slip rates at 18–150 °C. *Geology* 41, 863–866.
- Verberne, B.A., Spiers, C.J., Niemeijer, A.R., De Bresser, J.H.P., De Winter, D.A.M., Plümpner, O., 2013b. Frictional properties and microstructure of calcite-rich fault gouges sheared at sub-seismic sliding velocities. *Pure Appl. Geophys.* <http://dx.doi.org/10.1007/s00024-013-0760-0>.
- Wong, T.-f., Zhao, Y., 1990. Effects of load point velocity on frictional instability behavior. *Tectonophysics* 175, 177–195.
- Xu, X., Wen, X., Yu, G., Chen, G., Klinger, Y., Hubbard, J., Shaw, J., 2009. Coseismic reverse- and oblique-slip surface faulting generated by the 2008 Mw 7.9, Wenchuan earthquake, China. *Geology* 37 (6), 515–518.
- Yasuhara, H., Marone, C., Elsworth, D., 2005. Fault zone re-strengthening and frictional healing: the role of pressure solution. *J. Geophys. Res.* 110, B06310. <http://dx.doi.org/10.1029/2004JB003327>.
- Zhang, P., Wen, X., Shen, Z., Chen, J., 2010. Oblique, high-angle, listric reverse faulting and associated development of strain: the Wenchuan earthquake of May 12, 2008, Sichuan, China. *Annu. Rev. Earth Planet. Sci.* 38, 353–382.
- Zhang, X., Spiers, C.J., Peach, C.J., 2010. Compaction creep of wet granular calcite by pressure solution at 28 °C to 150 °C. *J. Geophys. Res.* 115, B09217. <http://dx.doi.org/10.1029/2008JB005853>.